Sputtering pressure influence on growth morphology, surface roughness, and electrical resistivity for strong anisotropy beryllium film*

Luo Bing-Chi(罗炳池)[a)b)], Li Kai(李 恺)[a)b)], Kang Xiao-Li(康晓丽)[a)], Zhang Ji-Qiang(张吉强)[a)], He Yu-Dan(何玉丹)[a)], Luo Jiang-Shan(罗江山)[a)†], Wu Wei-Dong(吴卫东)[a)b)], and Tang Yong-Jian(唐永建)[a)]

[a)] *Research Center of Laser Fusion, China Academy of Engineering Physics, Mianyang* 621900, *China*
[b)] *Science and Technology on Plasma Physics Laboratory, Mianyang* 621900, *China*

(Received 27 September 2013; revised manuscript received 12 December 2013; published online 10 April 2014)

The strong anisotropy beryllium (Be) films are fabricated at different sputtering pressures by direct current magnetron sputtering. With the increase of pressure, the deposition rate of Be film first increases, and when the pressure exceeds 0.8 Pa, it gradually descends. The X-ray diffraction analysis indicates that Be film is of α-Be phase, its surface always reveals the (101) crystal plane possessing the low surface energy. As for the growth morphology of Be film, the surface is mainly characterized by the fibrous grains, while the cross section shows a transition from a columnar grain to a mixed grain consisting of a cone-shaped grain and a columnar grain as the sputtering pressure increases. The large grain fraction decays exponentially from 75.0% to 59.3% with the increase of sputtering pressure p, which can improve the grain size uniformity. The surface roughness increases due to the insufficient atom diffusion, which is comparable to its decrease due to the etching effect at $p < 0.8$ Pa, while it increases drastically at $p > 0.8$ Pa, and this increase is dominated by the atom diffusion. The electrical resistivity values of Be films range from 1.7 μΩ·m to 2.7 μΩ·m in the range 0.4 Pa–1.2 Pa, which is 50 times larger than the bulk resistivity.

Keywords: magnetron sputtering, growth morphology, Be films, electrical resistivity

PACS: 68.55.–a, 68.55.J–, 68.55.Nq **DOI:** 10.1088/1674-1056/23/6/066804

1. Introduction

With the development of laser inertial confinement fusion (ICF), it is found that the beryllium films not only improve the implosion speed due to their good ablation properties, but also tolerate the larger roughness for the the D–T ice layer and control the Rayleigh–Taylor instability growth. Consequently, Be films are preferred to be used as the ignition target materials for the ICF experiments,[1–8] which is another important application for the beryllium besides serving as the X-ray window material. However, due to the fact that Be material has a poor ductility and large residual stress, it is difficult to fabricate the high quality Be films to meet the target design requirements, which restricts its application in the field of ICF. Thus, many fundamental properties of Be films need to be investigated.

The beryllium crystal lattice is of a hexagonal-close-packed structure, and has the lowest c-to-a ratio value in all the hexagonal-close-packed metals. The morphology and physical properties of Be film are different from those of other metals. Recently, the morphologies and physical properties of various film, such as pure metal films, oxide thin films, and alloy films[9–12] have been extensively studied, but little attention has been paid to the Be films. For the Be materials, the attention was focused mainly on the areas of the bulk materials founding, milling, bonding, and machining.[13–18]

The sputtering pressure is one of the important parameters for the film fabrication, and has a remarkable influence on the microstructure of metal thin films, such as the grain orientation, crystal structure, grain size, and grain distribution. However, its effect is still unclear on the property of Be film with strong anisotropy. The objective of this paper is to prepare the Be films by the DC magnetron sputtering technique, investigate the intrinsic relationships, such as the relationship of sputtering pressures with microstructure, and the relationship of sputtering pressures with surface roughness, grain size, and electrical resistivity. Finally, the obtained results provide a technique that supports fabricating high quality Be films.

2. Experimental details

The Be films were prepared by the DC magnetron sputtering technique. Four round magnetrons were equipped with a Be target 76 mm in diameter, positioned symmetrically around the center of the chamber. The discharge took place in a high purity argon gas (99.999 at.%) at a total pressure ranging from 0.4 Pa to 1.2 Pa. Before the deposition, the Si (100) substrates were boiled in the potassium dichromate solution for 5 min–10 min, and then washed by distilled water. Afterwards, the Si

*Project supported by the National Natural Science Foundation of China (Grant No. 11204280).
†Corresponding author. E-mail: jiangshanluo@caep.ac.cn
© 2014 Chinese Physical Society and IOP Publishing Ltd

substrates were cleaned by ultrasonic cleaning in an acetone solution for about 10 min, and then were etched in diluted hydrofluoric acid (5%) to remove the native oxide for about 30 s. Finally, the Si substrate was dried by the nitrogen blowing and fixed on the substrate holder in the sputtering chamber.

The target gun shutters and substrate shutter were closed during the pre-sputtering about 20 min. This aimed at etching the beryllium oxide on the Be target surfaces and cleaning the Si substrate surface. As is well known, the film microstructure, surface roughness, and physical properties are sensitive to the sputtering parameters. Therefore, they were adjusted and controlled strictly in the present experiment. The system was evacuated to a base pressure of 5.0×10^{-8} Pa. The pure Be (99.0 at.%) was used as the sputtering target. The distance between the substrate and Be targets was set to be $\sim$ 110 mm. The coating normally took place at 40 sccm of Ar gas flow and the Be guns operated at 60 W. During the deposition, all the shutters were open, and the sputtering time was accurately controlled to be 4 h by a computer.

The phase composition, microstructure, surface roughness, and electrical resistivity were determined using X-ray diffraction (XRD), a scanning electron microscope (SEM), a stylus-type surface profiler, and a four-point probe resistivity tester, respectively.

3. Results and discussion

3.1. Deposition rate

Figure 1 exhibits the variation of the deposition rate of beryllium on the Si (100) substrate with sputtering pressure. The deposition rate increases from 6.7 nm/min to 6.9 nm/min with pressure increasing from 0.4 Pa to 0.8 Pa, and then decreases gradually to 6.0 nm/min at 1.2 Pa.

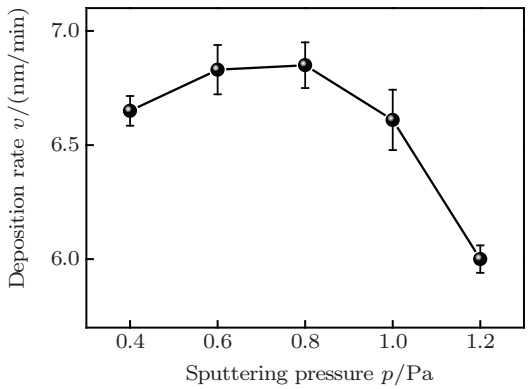


Fig. 1. Deposition rate of Be film versus sputtering pressure.

From the molecule kinematics viewpoint, the relationship between the molecule mean free path λ and sputtering pressure p is described as[19]

$$\lambda = k_{\mathrm{B}}T/\sqrt{2}\pi d^2 p, \tag{1}$$

where k_{B} is the Boltzmann constant, 1.38×10^{-23} J·K^{-1}; T is the gas molecule temperature, 573 K; d is the molecular diameter, about 0.376 nm. In the light of Eq. (1), the molecule mean free path is inversely proportional to the sputtering pressure. Obviously, the collision time between Be atoms and Ar atoms will increase with the enhancement of the sputtering pressure.

During the sputtering deposition, the possible Ar gas ionizations are listed as follows:

$$\mathrm{e} + \mathrm{Ar} \rightarrow \mathrm{Ar}^* + \mathrm{e}, \tag{2}$$

$$\mathrm{e} + \mathrm{Ar}^* \rightarrow \mathrm{Ar}^+ + 2\mathrm{e}, \tag{3}$$

$$\mathrm{e} + \mathrm{Ar} \rightarrow \mathrm{Ar}^+ + 2\mathrm{e}. \tag{4}$$

It can be seen that there are the Ar ions and metastable excited Ar* atoms according to expressions (2)–(4). When the sputtering pressure increases from 0.4 Pa to 0.8 Pa, the mean free path λ of Ar gas calculated from Eq. (1) decreases from 30 mm to 15 mm, which suggests that the particle scattering degree increases. While the ionization density of Ar gas increases with the rise of sputtering pressure, the deposition rate of Be film is enhanced due to the greater particle number. Here, although the particle scattering degree increases and the mean free path decreases, it cannot prevent the deposition rate from increasing. Accordingly, when the sputtering pressure is below 0.8 Pa, its growth results in an increase of the deposition rate. When the sputtering pressure exceeds 0.8 Pa, the mean free path is less than 15 mm, the collision probability between Be and Ar particles increases sharply, and the number of particles arriving at the substrate decreases. Although the sputtering pressure increases the number of sputtering particles, it cannot increase the deposition rate. Therefore, the deposition rate is mainly dominated by the mean free path at the higher sputtering pressure.

The sputtering pressure enhancing has both a positive contribution and a negative contribution to the deposition rate due to the increase of both the sputtering particle number and the scattering degree. When the sputtering pressure is about 0.8 Pa, the deposition rate has a maximal value of 6.9 nm/min.

3.2. Phase composition

The X-ray diffraction patterns for Be films grown on the Si (100) substrates in the pressure range from 0.4 Pa to 1.2 Pa are shown in Fig. 2. The Be films are mainly of α-Be phase. Their diffraction peaks are very sharp, and the intensity of the (101) peak is stronger than those of other peaks. It indicates that the (101) crystal facet possessing the lower surface energy always appears in the surface. The intensities of the other peaks change weakly with the increase of the sputtering pressure. In addition, the (101) peak of BeO occurs at 0.4 Pa and 1.2 Pa, which suggests that some amount of BeO exists in the Be films.

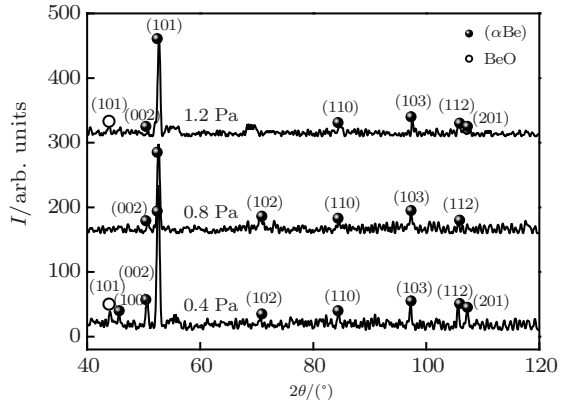


Fig. 2. XRD patterns of Be films at the different sputtering pressures.

3.3. Growth morphology

The lattice constant of monocrystal Si is 0.5431 nm, while Be lattice constant is $a = 0.2281$ nm and $c = 0.3578$ nm. The large difference between them prevents perfect hexagonal beryllium crystal grain or monocrystal Be from growing on a Si (100) substrate. The surface and cross-section morphologies of Be films observed by the SEM are characterized by the coarsening fibrous grains with pressure increasing. The adjacent grain boundaries form an angle of 120°, as illustrated in Figs. 3(a)–3(c). It is reasonable to infer that the grain is a corner of the hexagonal crystal. There are remarkable varieties of grain sizes and they are distributed on the film surface.

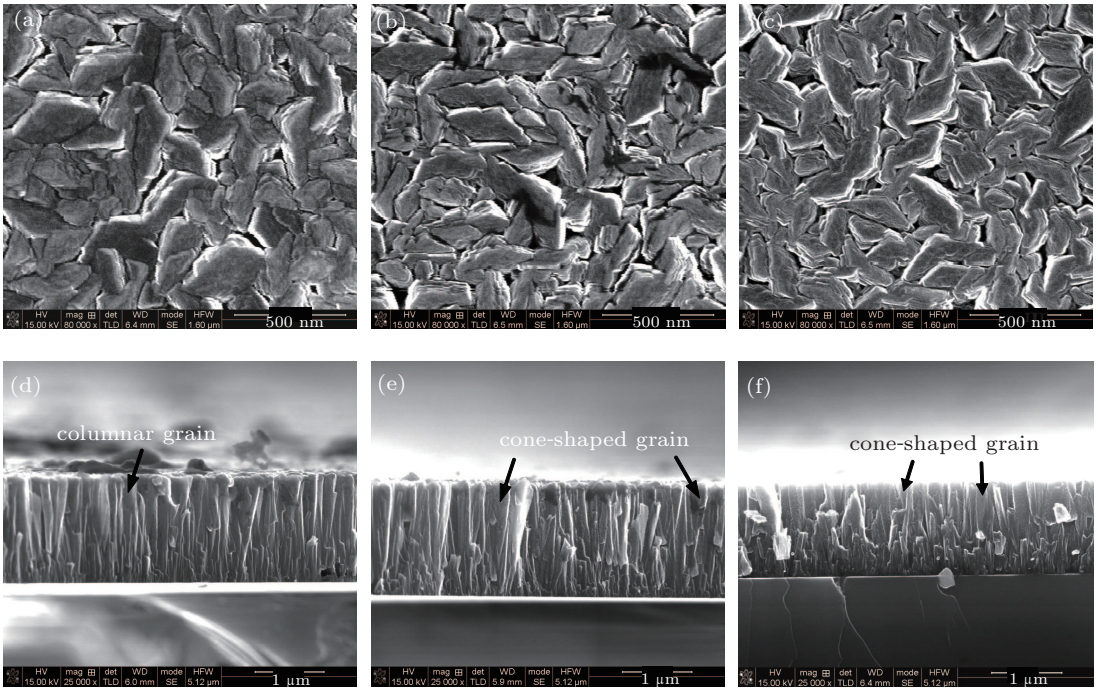


Fig. 3. Surfaces and cross-section morphologies of Be films at the different sputtering pressures. Panels (a), (b), and (c) show the surfaces morphologies at sputtering pressures of 0.4, 0.8, and 1.2 Pa, respectively, and panels (d), (e), and (f) show their corresponding cross-section morphologies.

The cross section is characterized by the coarsening columnar grains, as shown in Figs. 3(d)–3(f). With the increase of the sputtering pressure, the cross section shows a transition from the columnar grains to the mixed grains consisting of the cone-shaped and columnar grains. The cross section displays the columnar grains below 0.6 Pa. In the initial nucleation process, the Be film grows in the form of fine columnar grains with a diameter of 30 nm and a length of 130 nm. When the film thickness reaches 1.6 μm, the columnar grains can grow up to 162 nm in diameter. A new depositing atom attaches to an available grain, and the grain grows up gradually with the increase of deposition time. When the sputtering pressure is in the range 0.8 Pa–1.2 Pa, the cross section consists of the cone-shaped and columnar grains with an average grain size of $\sim$ 140 nm.

In order to further study the intrinsic relations of grain sizes and distribution with sputtering pressure, the quantitative metallographic method is used. The average grain size G_a is defined as the ratio of the total scanning length to the grain number, and the large grain fraction F is the ratio of the large grain number (their grain size exceeds G_a) to the total grain number. The G_a decreases from 189 nm to 148 nm in the range 0.4 Pa–1.0 Pa, and increases slightly to 161 nm at 1.2 Pa as indicated in Fig. 4. The F decreases gradually from 75.0% to 59.3% with the rise of the sputtering pressure. Clearly, the sputtering pressure can improve the grain uniformity and be favorable to the grain refinement.

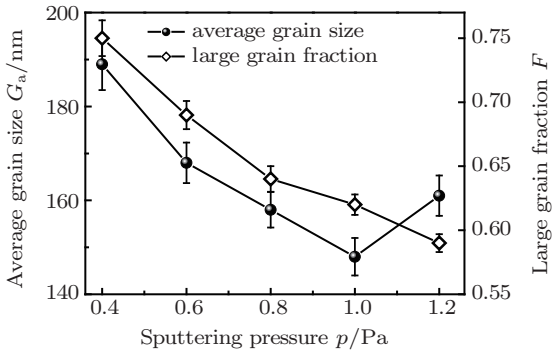


Fig. 4. Average grain size and large grain fraction of Be films versus sputtering pressure.

Be has a high melting point, $T_m = 1287$ °C. The substrate temperature T_s is about 60 °C during the deposition, and the ratio of T_s/T_m is about 0.21. When the sputtering pressure is in the range 0.4 Pa–1.2 Pa, the morphology belongs to the zone T (transition) region on the basis of Thornton classification. The films have the dense fibrous structures and their surfaces are very smooth. However, the morphologies for strong anisotropy Be films are different from that grown in the T region. Although the film surface consists of fibrous grains, the grains are rather large.

3.4. Surface roughness

The root-mean-square roughness R_q and the average roughness R_a have a similar dependence on the sputtering pressure, as plotted in Fig. 5. The surface roughness values of strong anisotropy Be films have no evident changes in the range 0.4 Pa–0.8 Pa. R_q is about 14 nm, and R_a is about 11 nm. When the sputtering pressure exceeds 0.8 Pa, both R_q and R_a increase sharply. The R_q is 25 nm and R_a is 17 nm at 1.2 Pa. Due to the shadowing effect during the deposition, the high points on the growing surface receive more sputtering flux than the valleys, the surface roughness will increase with the sputtering pressure, especially at the higher sputtering pressure.

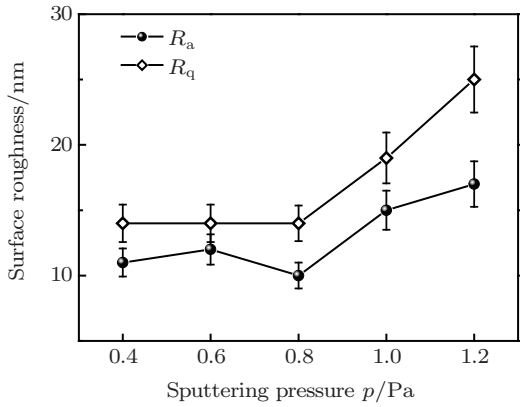


Fig. 5. Surface roughness values of Be films versus sputtering pressure.

On the one hand, the deposited Be particles are scattered by Ar^+ ions, metastable atom Ar^*, and Ar atoms with the increasing of sputtering pressure. The mean-free-path and kinetic energy of incoming Be particles will decrease, and the atom diffusion ability on the substrate will weaken. It will lead to void formation due to insufficient atom diffusion distance. Thus, the surface roughness will increase. At the same time, the sputtering particles have an etching effect on the Be film surface. This effect in a peak region is stronger than in a valley region. Therefore, the more sputtering particles, the better the surface smoothing and finishing are. According to experimental results, the surface roughness changes weakly in the range 0.4 Pa–0.8 Pa. It indicates that the roughness increase by the insufficient atom diffusion is comparable to its decrease by the etching effect. When the sputtering pressure exceeds 0.8 Pa, the surface roughness increases sharply, which suggests that the surface roughness is dominated by the atom diffusion and mobility ability.

3.5. Electrical resistivity

When the collision of the free electrons takes place, they lose their directional velocity given by the outer electric field. The crystal lattice atoms move around their balanceable positions. Their unregulated array will result in the collisions of electron with crystal lattice, impurities, crystal boundary, surface, etc. The electrical resistance of metal thin film results from two contributions, i.e., the intrinsic resistance deriving from the heat vibration of the crystal lattice atoms and the residual resistance originating from the impurity atoms, vacancies, and dislocations. For most metals, the intrinsic resistance is larger than the residual resistance at room temperature.

The electrical resistivity ρ is measured by the four-point probe resistivity tester, and it is expressed as[20]

$$\rho = \frac{\pi}{\ln 2}\frac{V}{I}\delta F, \tag{5}$$

where V is the probe voltage, I is the probe current, and δ is the film thickness. If the distance between probe and film edge is three times larger than the probe distance, the modified factor $F = 1$.

Figure 6 shows the electrical resistivity versus sputtering pressure. When the sputtering pressure is below 0.8 Pa, the electrical resistivity of Be film always keeps the ascending trend, and increases from 1.7 μΩ·m to 2.7 μΩ·m within a measurement error of 3%, while the electrical resistivity descends to 2.1 μΩ·m at 1.2 Pa. Compared with the Be bulk resistivity of 4.0×10^{-8} Ω·m, the film electrical resistivity is 50 times larger than the bulk resistivity.

It is found that the electrical resistivity ρ depends on average grain size G_a, as indicated in Fig. 7. With the increase of grain size, the electrical resistivity of Be film decreases first conspicuously, and then slowly. It can be reasonably deduced that the average grain size G_a directly influences the film resistivity. The smaller the grain size, the more atoms are located

at the crystal boundary. Accordingly, the electrical resistivity of Be films will increase due to the collision of free electrons on the crystal boundary.

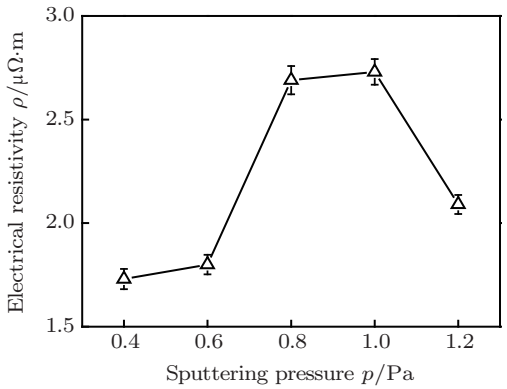


Fig. 6. Electrical resistivity of Be film versus sputtering pressure.

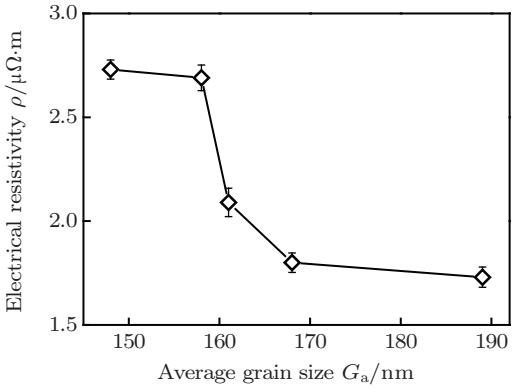


Fig. 7. Electrical resistivity of Be film versus average grain size.

4. Conclusions

In this paper, it is found that as the sputtering pressure increases, the deposition rate of Be film increases from 6.7 nm/min to 6.9 nm/min, and then decreases gradually to 6.0 nm/min. The increase of the sputtering pressure enhances the sputtering particle number, and it reduces the particle mean-free-path as well. The deposition rate of Be film is determined by both of them. Be film with a strong anisotropic property is mainly of α-Be phase, and the film surface always presents the (101) crystal plane possessing the lower surface energy. Although the sputtering conditions correspond to Thornton's T zone, there exist some differences in morphology. The film surface is characterized by a coarsening fibrous grain, and the cross section shows a transition from a columnar grain to a mixture grain consisting of a cone-shaped grain and columnar grain with the increase of sputtering pressure. The G_a decreases from 189 nm to 148 nm in the pressure range 0.4 Pa–1.0 Pa, and the G_a slightly increases to 161 nm at 1.2 Pa. The film surface roughness is almost constant below 0.8 Pa, while it increases sharply beyond 0.8 Pa. The surface roughness is dominated by the atomic diffusion ability and plasma etching effect. The electrical resistivity of Be films increases gradually from 1.7 μΩ·m to 2.7 μΩ·m below 0.8 Pa, and descends to 2.1 μΩ·m at 1.2 Pa. The electrical resistivity decreases as G_a increases, owing to the fewer collisions of free electrons with the crystal boundary.

Acknowledgment

The authors are grateful to Mr. Zeng Yong, Mr. Zhang Jian-Bo, Mrs. Tan Xiu-Lan, and Dr. Shen Chang-Le for their beneficial discussion.

References

[1] Haan S W, Herrmann M C and Amendt P A 2006 *Fusion Sci. Technol.* **49** 553
[2] Xu H W, Alford C S, Cooley J C, Dixon L A, Hackenberg R E, Letts S A, Moreno K A, Nikroo A, Wall J R and Youngblood K P 2007 *Fusion Sci. Technol.* **51** 547
[3] Haan S W, Amendt P A and Callahan D A 2007 *Fusion Sci. Technol.* **51** 509
[4] Moreno K A, Eddinger S and Fong J 2009 *Fusion Sci. Technol.* **55** 349
[5] Haan S W, Callahan D A and Edwards M J 2009 *Fusion Sci. Technol.* **55** 227
[6] Montgomery D S, Nobile A and Walsh P J 2004 *Rev. Sci. Instrum.* **75** 3986
[7] Davydov D A, Kholopova O V and Kolbasov B N 2007 *J. Nucl. Mater.* **367** 1079
[8] Nikroo A, Chen K C, Hoppe M L, Huang H, Wall J R, Xu H, McElfresh M W, Alford C S, Cook R C, Cooley J C, Fields R, Hackenberg R, Doerner R P and Baldwin M 2006 *Phys. Plasmas* **13** 056302
[9] Blum V, Rath Ch, Müller S, Hammer L and Heinz K 1999 *Phys. Rev. B* **59** 15966
[10] Singh S, Thiyagarajan P, Kant K M, Anita D, Thirupathiah S, Rama N, Tiwari B, Kottaisamy M and Rao M S R 2007 *J. Phys. D: Appl. Phys.* **40** 6312
[11] Chou C Y, Yao Y D, Kuo P C, Cheng K W and Yu C 2006 *J. Magn. Magn. Mater.* **304** e103
[12] Yao X F, Wang J P, Zhou T J and Chong T C 2005 *J. Appl. Phys.* **93** 8310
[13] Tikhinskij G F, Stoev P I, Papirov I I, Babun V A and Vasilév A A 1996 *J. Nucl. Mater.* **233** 828
[14] Song D J, Zhang X M and Hu Q 2006 *Mater. Rev.* **20** 66
[15] Wang H P, Chang J and Wei B 2009 *J. Appl. Phys.* **106** 033506
[16] Ma X B, Wang H P, Zhou K, Chang J and Hong Z Y 2013 *Appl. Phys. Lett.* **103** 104101
[17] Zhu Z W, Gao X D, Zhang Z B, Piao Y H, Hu C, Zhang D W and Wu D P 2012 *Chin. Phys. B* **21** 087304
[18] Zhang L S, Yu H F and Guo Y Q 2012 *Acta Phys. Sin.* **61** 016101 (in Chinese)
[19] Lutišan J and Cvengroš J 1995 *Chem. Eng. J.* **56** 39
[20] Xie H B 1999 *Vacuum* **3** 37